Áron Ágoston[1]
Lilla Balassa[1]
Ágota Deák[1]
Gergely Ferenc Samu[1]
Szabolcs Péter Tallósy[2]
Gyöngyi Gombár[1]
László Janovák[1,*]

Photocatalytic and Antimicrobial Activity of Sulfur-Functionalized TiO_2-Containing Composite Films

Facile sulfation of TiO_2 semiconductor photocatalyst was achieved by a simple grinding and calcination method using elemental sulfur from desulfurization of petroleum. The successful sulfation of the prepared visible-light-active photocatalyst was also proved by infrared and X-ray photoelectron spectroscopic measurements. Photocatalytic tests revealed that the most efficient member of the series has higher photocatalytic activity than TiO_2 in the photodegradation of formic acid under both UV and visible-light activation. Moreover, the improved electrokinetic and water dispersibility behaviors of the sulfur-modified photocatalyst allowed the preparation of polyacrylate-based photoreactive thin films with increased photocatalytic activity, strong antimicrobial properties, and improved mechanical behavior.

Keywords: Antibacterial coatings, Enhanced suspension stability, Petroleum byproducts, Sulfated titania, Visible-light activity

Received: October 12, 2022; *revised:* December 20, 2022; *accepted:* January 17, 2023

DOI: 10.1002/ceat.202200489

Supporting Information available online

1 Introduction

Heterogeneous photocatalysis remains very popular among researchers, since it has a wide range of applicability [1]. Titanium dioxide (TiO_2) is a much studied photocatalyst worldwide [2, 3], because of its excellent properties, e.g., high photocatalytic activity, inert nature, high stability, low toxicity, and low cost [2, 4]; hence, TiO_2 is applied in environmental and many other fields [2]. Considering that ultraviolet (UV) photons in particular can activate TiO_2 (band gap: ca. 3.0 eV for rutile and 3.2 eV for anatase) [5], attempts are made to modify this photocatalyst to extend its absorption spectrum. A visible-light-active photocatalyst can be used more widely and it would be cheaper, because of the availability of sunlight (ca. 45 % visible and ca. 4–5 % UV light) [6]. Catalyst doping or modification is an outstanding technique to improve the activity in the visible region; hence, researchers are doping TiO_2 or modifying its surface with various elements (S, N, C, Se, Fe, Cu) [7–10].

Since the report on visible-light-active sulfur-doped TiO_2 (S-TiO_2) by Umebayashi et al. [11], it has become an intensively researched topic. The S^{6+} ion impurities in the crystal lattice of TiO_2 result in a smaller band gap [11], and the SO_4^{2-} ions on the surface have a synergistic effect, too, so it acts as an efficient electron trap [12]. Many sulfur sources for doping or surface modification have been reported, e.g., sulfuric acid and dissolved elemental sulfur [13, 14]. In this work, dissolved elemental sulfur was used for the modification of the TiO_2 surface by a heat treatment method. This surface modification with sulfur is advantageous, because sulfur is available in large quantities due to the desulfurization of petroleum.

One of the main areas of novel photocatalysts is self-cleaning surfaces that degrade both living and nonliving contaminants and can be excited by sunlight, without any other light source. An excellent self-cleaning and antibacterial surface can be made with a visible-light-excitable photocatalyst and a suitable binder. Thus, the development of photocatalysts is very important from a microbiological point of view. A sunlight-excitable surface with the above-mentioned advantageous properties would be useful in many areas.

This work reports the preparation, characterization, photocatalytic activity, hydroxyl-radical-producing ability, and antimicrobial efficiency of a sulfur-modified TiO_2 photocatalyst. It also presents the preparation of a photocatalytically active self-cleaning and antimicrobial surface that can be excited by sunlight and the mechanical properties of the surface.

[1]Áron Ágoston, Lilla Balassa, Dr. Ágota Deák, Dr. Gergely Ferenc Samu, Gyöngyi Gombár, Dr. László Janovák (janovakl@chem.u-szeged.hu)
Department of Physical Chemistry and Materials Sciences, University of Szeged, Rerrich B. t. 1, H-6720 Szeged, Hungary.

[2]Dr. Szabolcs Péter Tallósy
Institute of Clinical Microbiology, Faculty of Medicine, University of Szeged, Semmelweis u. 6, H-6725 Szeged, Hungary.

2 Materials and Methods

2.1 Catalyst Preparation

During catalyst synthesis a reported preparation procedure was improved [12]. In this study five surface-modified TiO_2 materials (S-TiO_2-*X*) were synthesized from commercially available TiO_2 (Aeroxide P25) by a facile thermal method. For 1.5 atom % sulfur concentration (S-TiO_2-1), 0.06 mg of dissolved sulfur [1 mL of a 0.0602-g L^{-1} stock solution of sulfur in benzene (≥ 99.7 %, VWR Chemicals)] was added to 1 g of TiO_2, and the mixture was ground in an agate mortar. The mixture was dried at 120 °C for 4 h. The grinding process was repeated three times and the obtained product was calcined at 200 °C for 4 h. In the case of S-TiO_2-2–5, the volume of added sulfur-containing benzene solution was increased from 2 to 5 mL, respectively. The adjusted nominal sulfur contents of the materials are listed in Tab. 1.

Table 1. Nominal sulfur contents and binding energies for the various TiO_2 materials from the fits of the Ti 2p region.

Material	S [atom %]	S [wt %]	Ti $2p_{3/2}$ [eV]	Ti $2p_{1/2}$ [eV]	ΔE [eV]
TiO_2	0	0	458.30	464.15	5.85
S-TiO_2-1	1.5	6.02×10^{-3}	458.27	464.07	5.80
S-TiO_2-2	3	1.20×10^{-2}	458.32	464.97	5.65
S-TiO_2-3	4.5	1.81×10^{-2}	458.57	464.34	5.77
S-TiO_2-4	6	2.41×10^{-2}	458.42	464.07	5.65
S-TiO_2-5	7.5	3.01×10^{-2}	458.51	464.31	5.80

2.2 Preparation of Photocatalytic Thin Films

For further experiments the photocatalyst particles were immobilized in a polyacrylate binder matrix [poly(ethyl acrylate-*co*-methyl-methacrylate), Evonik Industries, Germany). The thin films were prepared by spray coating on the surface of glass plates with a surface area of $A = 25\ cm^2$ (5 × 5 cm). During film preparation a 5-g L^{-1} aqueous photocatalyst/polymer dispersion consisting of 90 wt % photocatalyst and 10 wt % polymer was evenly layered on the glass plates with a gravity feed airbrush (ChroMax BD-203) to obtain a surface coverage of 1 mg cm^{-2}. To prevent any undesirable reactions during the spray coating process, an inert nitrogen gas flow was used at a pressure of 3.5 bar.

2.3 Characterization

X-ray diffraction (XRD) measurements were carried out with a Philips powder XRD instrument (PW 1820 goniometer, PW 1830 generator, $Cu_{K\alpha}$ radiation: wavelength $\lambda^{1)} = 0.1542$ nm, 40–50 kV, 30–40 mA, $2\theta = 2$–70°, $T = 25.0 \pm 0.5$ °C) to determine the crystalline properties.

To record the Fourier transform infrared (FTIR) spectra of the photocatalysts, a Jasco FTIR 4700 spectrometer was used. The spectra were measured between 4000 and 500 cm^{-1} with a resolution of 1 cm^{-1}.

X-ray photoelectron spectroscopy (XPS) was carried out with a SPECS instrument with PHOIBOS 150 MCD 9 hemispherical analyzer. During the measurements, fixed analyzer transmission mode was used with a pass energy of 40 eV, and AlK_α radiation of a dual-anode X-ray gun was used as the excitation source. The X-ray source was operated at a power of 150 W. The spectra were analyzed with the CasaXPS software package. For the adventitious carbon (284.8 eV) present on the surface of the samples, charge referencing was performed.

The optical characterization of the S-TiO_2-*X* samples was carried out with a CHEM2000 UV-VIS (USB2000+UV-VIS, Ocean Optics Inc.) spectrophotometer, equipped with an integrating sphere. The diffuse-reflectance (DR) UV-visible (Vis) spectra of the samples were recorded and the corresponding band gap energies were determined by the Kubelka-Munk method [15].

The specific surface areas of the samples were determined by the Brunauer-Emmett-Teller (BET) method from N_2 adsorption isotherms (77 ± 0.5 K) with a Micromeritics Gemini 2375 Surface Area Analyzer.

For hydrodynamic stability the zeta potentials ζ of the aqueous photocatalyst dispersion were determined with a Horiba nanoPartica SZ-100 nanoparticle analyzer in a carbon-coated electrode cell. The concentration of the aqueous suspensions was 0.01 wt % before the measurements, and the suspensions were sonicated for 5 min for homogeneity. A Horiba SZ-100 zeta cell was used.

The elemental distribution and the titanium content as well as the homogeneity of the TiO_2- and S-TiO_2-2-containing polyacrylate films were determined by energy-dispersive X-ray (EDX) measurements with a Hitachi S-4700 electron microscope. Before the measurements, the films with 90 % photocatalyst content were activated by UV.

2.4 Photocatalytic Activity Measurements

The photocatalytic activities of the S-TiO_2-*X* samples were measured at room temperature on both solid/liquid and solid/gas interfaces.

In suspension (solid/liquid interface) photocatalytic tests, formic acid (98–100 %, Sigma Aldrich) was used as model pollutant, and the experiments were performed in an open glass reactor with a diameter of 15 cm. The photocatalytic activities were measured separately under UV light (λ_{max} = 365 nm; Fig. S1A in the Supporting Information) and under visible light (λ_{max} = 610 nm; Fig. S1B) with low UV content. The light sources were fixed at a distance of 5 cm from the surface of the irradiated aqueous suspensions. The volume of the continuously stirred reaction mixture was 70 mL, and the decreasing concentration of the model pollutant was followed with a Shimadzu

1) List of symbols at the end of the paper.

UV-1800 UV-Vis spectrophotometer. The photocatalyst concentration was 0.05 wt %, while the initial formic acid concentration was 0.05 vol % (1.24×10^{-5} mol L^{-1}). To ensure adsorption equilibrium, before irradiation the suspension was kept in the dark for 30 min. 3.5-mL samples were collected, and before spectrophotometric analysis the samples were centrifuged and filtered through a 0.1-μm Millex-VV PVDF filter.

For the gas/solid interface, ethanol (100 %, Molar Chemicals Kft.) vapor was used, and the experiments were performed in a circulation reactor with a volume of 165 mL. The stainless steel photoreactor was covered with a quartz plate. A visible light source was used during the degradation process. The light source was fixed at a distance of 5 cm from the surfaces. After injection of absolute ethanol and water, the relative humidity was ca. 70 %, and the initial concentration of ethanol vapor was 0.36 mmol L^{-1}. Before irradiation, the system was kept in the dark for 30 min to ensure adsorption equilibrium on the surface of the films. The collected samples were analyzed with a Shimadzu GC14B gas chromatograph equipped with flame ionization and thermal conductivity detectors.

2.5 Detection of Hydroxyl Radicals

The production of hydroxyl radicals was followed through 7-hydroxycoumarin formation on the photocatalytic thin films [16]. Before the measurements the 5 x 5 cm composite surface with 10 wt % polymer content was activated by UV light (UV-C lamp) for 30 min. Hydroxyl radical production capacity was measured on both the TiO_2- and S-TiO_2-2-containing samples. During the measurements, the initial concentration of coumarin (> 99 %, Sigma) was 10^{-4} mol L^{-1} in 50 mL solution, and a visible light source was used (Fig. S1B). The photocatalytic film was placed in the center of the solution, and the surface of the solution was at a distance of 5 cm from the light source. The 7-hydroxycoumarin concentration change was followed with a HORIBA Jobin Yvon Fluoromax-4 spectrofluorometer. During the measurements the excitation wavelength of 7-hydroxycoumarin was 345 nm and the detection wavelength was 453 nm.

2.6 Stability of Aqueous Suspensions

Aqueous suspensions of TiO_2 and S-TiO_2-2 were prepared in concentrations of 0.005 wt %, and 2.5 mL of the suspensions was poured into a cuvette with 1-cm path length. The sedimentation kinetic of the suspension was followed by absorbance measurement at 600 nm detection wavelength by a Gallenkamp SP 50 spectrophotometer.

2.7 Mechanical Stability of Photocatalytic Thin Films

The mechanical stability of the thin films was examined with a Taber Crockmeter (Model 418). The sample plates were clamped and were subjected to the alternating movement of an acrylic glass cylinder. One back and forth movement corresponds to one cycle, and the weight loss was measured as a function of the number of crocking abrasive cycles.

2.8 Microbiological Applications

The antimicrobial tests were completed according to modified EN ISO 27447:2009 standard using *Escherichia coli* ATCC 29522 reference strain obtained from international reference culture collection. Detailed measurements can be found in the Supporting Information.

3 Results and Discussion

3.1 Characterization

Fig. 1 shows the FTIR spectra of TiO_2 and S-TiO_2 samples in the range of 1000–2000 cm^{-1}. The strong band at 1647 cm^{-1} is the O–H bending vibration, which typically appears between 1660 and 1600 cm^{-1}, which came from adsorbed H_2O [17]. The intensity of the peak increases with increasing sulfate content. At 1415 cm^{-1} is the asymmetric stretching band of the S=O bond, which typically appears between 1415 and 1380 cm^{-1} [17]. At 1130 cm^{-1} is the S–O band, belonging to the bidentate SO_4^{2-} group, which binds to the Ti^{4+} ion [17]. Thus, based on these results, it can be concluded that sulfate groups are on the surface.

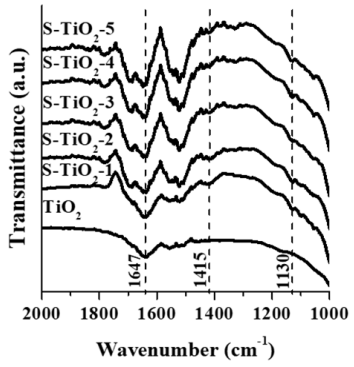

Figure 1. FTIR spectra of TiO_2 and S-TiO_2-*X*.

Next, XPS measurements were performed to study the surface composition of the sulfur-treated TiO_2 materials. The survey scans (Fig. S3) show similar chemical makeup for the samples, where the presence of carbon, titanium, oxygen can be identified. The presence of sulfur is not apparent on the surface of the samples, because of the small quantity (1.5–7.5 atom %) on the surface coupled with the relatively limited sensitivity of XPS to this element [18]. High-resolution scans were recorded for the different regions in the sample. The Ti 2p region (Fig. 2A) shows the exclusive presence of Ti^{IV} on all of the sample surfaces. In all cases, only one component was necessary to fit the high-resolution Ti 2p spectra, and the binding energies are summarized in Tab. 1. These determined binding energies correspond well to the binding energy range of Ti^{IV} in TiO_2 materials ($2p_{3/2}$ at 458.66 ± 0.3 eV with a peak

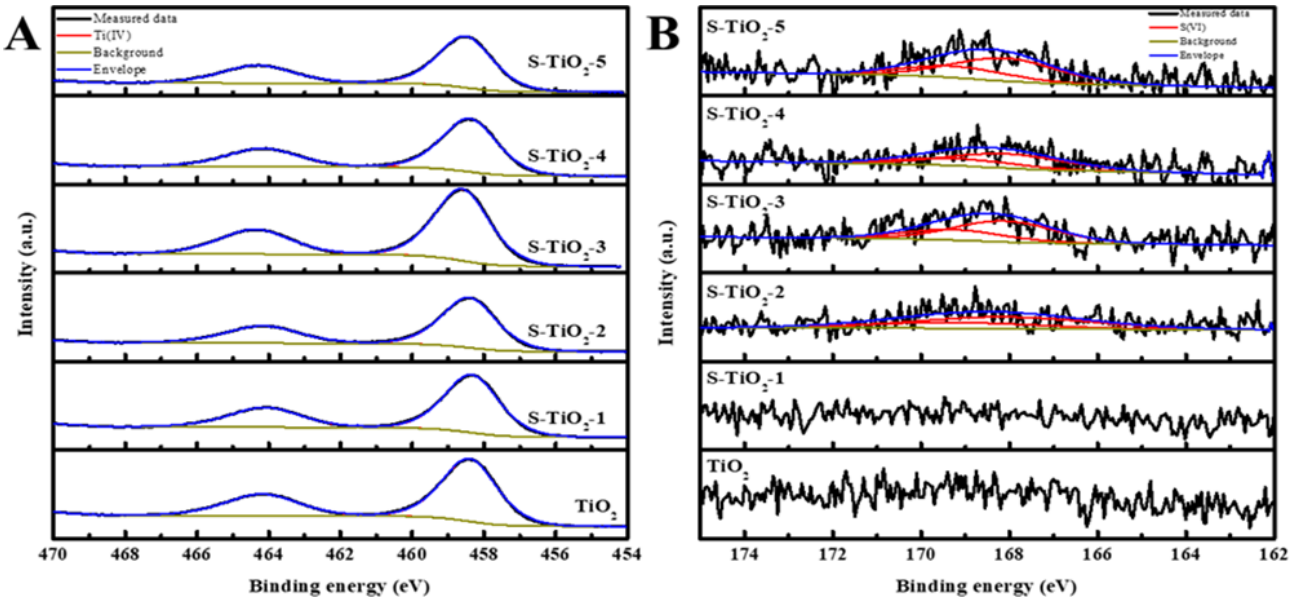

Figure 2. High-resolution XP spectra of the (A) Ti 2p and (B) S 2p regions of TiO_2 and S-TiO_2.

separation of ΔE = 5.66 eV) [19]. The high-resolution scan of the S 2p region (Fig. 2B) reveals the presence of sulfur in samples for which a larger amount of sulfur solution was used during synthesis. The binding energy of these sulfur species (S $2p_{3/2}$ ca. 168.10 eV) indicates that they are most likely in the +6 oxidation state, possibly originating from surface-bound sulfate (free-standing sulfate S $2p_{3/2}$ ca. 168.90 eV) [20].

The band gaps were calculated using the Kubelka-Munk equation from DR spectra [15]. Fig. S5 shows Kubelka-Munk representations of the S-TiO_2-2 and initial TiO_2 photocatalysts [15]. All the S-TiO_2-*X* samples show light absorption in the visible region. The calculated values are listed in Tab. 2, and they varied between 2.90 and 2.96 eV; therefore, these photocatalysts can be excited by visible light with 427 nm or shorter wavelengths. Although sulfated samples require roughly the same amount of energy to excite, sulfate only serves to trap the already excited electron, prolonging or preventing the recombination. Greater sulfate modification had no effect on the structure of the excitable region of the photocatalyst, and the differences between sulfated samples were smaller than those between sulfated samples and titanium dioxide. The sulfate group bound to the surface is considered to be a surface crystal defect from the point of view of the block phase, which can cause local, weak polarization due to the different electronegativity.

The specific surface areas and crystal sizes of the S-TiO_2-*X* samples are listed in Tab. 2. Surface modification did not change significantly the BET surface area or the crystal size, since the former varied between 42.3 (S-TiO_2-3) and 64.09 m^2g^{-1} (S-TiO_2-1), and the crystal size between 19.27 and 22.4 nm.

Next, it was studied how the presence of surface sulfate groups affects the electrokinetic properties of the samples. The zeta potentials indicate that the surface charges of the initial P25 TiO_2 photocatalyst particles (–28.6 mV at pH 6.63) decreased after sulfur modification, and the zeta potentials of the modified samples were around –70 mV (pH 5.70 ± 0.22), independent of the sulfur content, i.e., the surface sulfur content increased the surface charge of the initial TiO_2 (Fig. 3). Furthermore, this enhanced surface charge improved the colloidal stability in aqueous suspension.

This enhanced aqueous stability was demonstrated by simple sedimentation experiments (see Supporting Information).

Numerous investigations in the literature confirm the stability of the sulfate group on different photocatalyst surfaces, including TiO_2 surfaces [21–23]. The catalyst was dispersed both before and after usage, and the supernatant liquid was added to $Ba(OH)_2$ solution. No precipitate was produced, and the dispersion was also examined with a turbidity meter, which revealed that the solution remained clear.

Table 2. Band gaps E_g, excitation wavelengths, specific surface areas, and crystal sizes of TiO_2 and S-TiO_2-*X* samples.

Sample name	E_g [eV] by Kubelka-Munk	Excitation wavelength [nm]	Specific surface area [m^2g^{-1}]	Crystal size [nm]
TiO_2	3.20	387.75	53.00	20.26
S-TiO_2-1	2.95	420.29	64.09	19.27
S-TiO_2-2	2.91	427.53	52.64	22.39
S-TiO_2-3	2.95	420.29	42.30	19.34
S-TiO_2-4	2.96	418.87	51.70	21.27
S-TiO_2-5	2.92	424.60	49.88	22.39

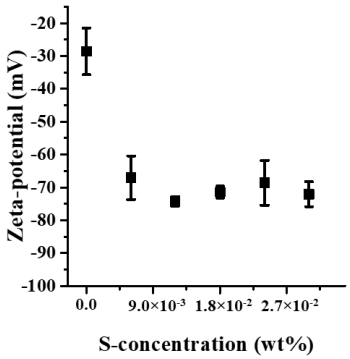

Figure 3. Zeta potentials of S-TiO_2-*X* aqueous dispersions as a function of increasing sulfur content.

3.2 Photocatalytic Properties in Aqueous Suspension

Since the surface-modified photocatalysts have smaller band gaps and higher water stability than commercial TiO_2, the question arose how this phenomenon manifests itself in the photocatalytic activity.

The adsorption experiments showed that the surface coverage of TiO_2 was 3.56×10^{-5} $mg_{HCOOH}\,g_{TiO2}^{-1}$ with 0.55 mg L^{-1} final equilibrium concentration of HCOOH, and the surface coverage of S-TiO_2-2 was 3.32×10^{-5} $mg_{HCOOH}\,g_{TiO2}^{-1}$ with the same HCOOH equilibrium concentration. These results showed similar adsorption abilities of photocatalysts for formic acid under the applied conditions.

The photocatalytic experiments started with the direct photolysis of formic acid without photocatalyst at the same formic acid concentration, and then commercial TiO_2 was used as reference photocatalyst. Finally, all the prepared S-TiO_2 photocatalysts were applied at the same concentration. The results are shown in Fig. 4A.

Of the synthesized photocatalysts, S-TiO_2-2 showed the highest photocatalytic activity. Next, all previous measurements were repeated with visible light as irradiation source (Fig. 4B). S-TiO_2-2 had the highest photocatalytic activity in this case as well, and all of the synthesized catalysts were better than TiO_2. Thus, the results reveal that the sulfur modification increased the photocatalytic activity under UV and under visible light. It is noticeable that some points of the control measurement are above $c/c_0 = 1$, which happened because the reactor was not closed; the increase of ca. 1 % proves that evaporation was not significant. This also confirms that the formic acid did not decompose without the presence of the photocatalyst.

3.3 Photocatalyst Immobilization and Characterization of the Composite Layers

Details of this topic can be found in the Supporting Information.

3.4 Detection of Hydroxyl Radicals Produced on the Surface of the Photoreactive Layer

The experiments were preceded by calibration of spectrofluorometer with 7-hydroxycoumarin (99 %, Aldrich) and the concentration dependence was linear over the range used (1×10^{-8} to 5×10^{-6} mol L^{-1}). In the absence of catalyst, 7-hydroxycoumarin cannot be formed by light irradiation, because 7-hydroxycoumarin is formed only in the reaction of coumarin with hydroxyl radicals.

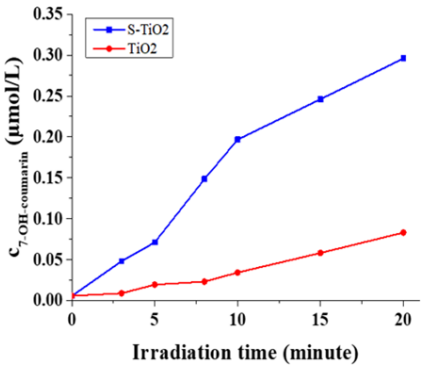

Figure 5. Production kinetics of 7-hydroxycoumarin from coumarin on the surface of TiO_2 and S-TiO_2-2 photocatalytic thin films (A = 25 cm^2, specific surface area: 1 mg cm^{-2}).

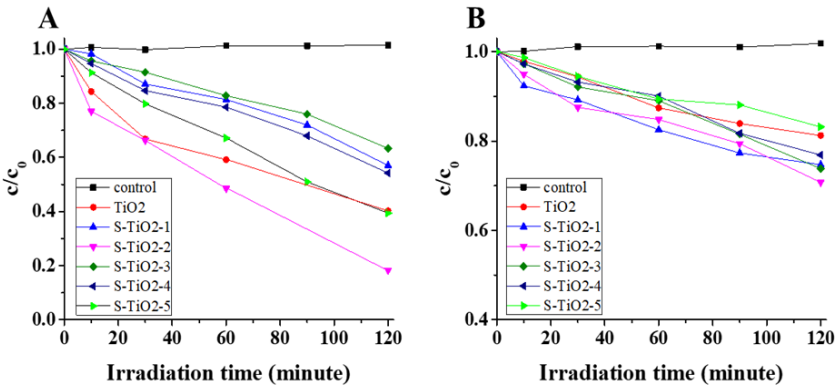

Figure 4. Photocatalytic activity of S-TiO_2-X photocatalysts and TiO_2 in suspension under UV (A) and visible-light (B) irradiation. *c*: concentration, c_0: initial concentration.

The formation kinetics of 7-hydroxycoumarin is shown in Fig. 5. The results indicate that the S-TiO_2-2 photocatalyst has better hydroxyl radical production capacity than unmodified TiO_2. The measured values show continuously increasing tendency in both cases, but after 20 min of irradiation the concentration of 7-hydroxycoumarin was 0.083 μmol L^{-1} in the case of TiO_2 and 0.296 μmol L^{-1} in the case of S-TiO_2-2. In other words, the sulfur-modified catalyst has higher hydroxyl radical generation capacity under the same conditions. This is certainly due to the smaller band gap (Tab. 1).

3.5 Microbiological Applications

The results of the microbiological experiments are shown in Fig. 6. After the antibacterial tests, it is clear that in the presence of S-TiO_2-2 photocatalyst there is a strong increase in the antibacterial effect compared to the control samples (polyacrylate binder without photocatalyst). The light intensity was 1.566 W m^{-2} during the experiment at this distance (60 cm). In the case of the control surface after 60 min of irradiation time, the initial bacterial count of 5.14 colony-forming units (CFU) did not change, whereas in the case of the S-TiO_2-2 photocatalytic thin film, inactivation was complete after 30 min. This means that the S-TiO_2-2-containing layer shows a strong antimicrobial effect under even relatively low irradiation, and thus it is suitable for antimicrobial purposes.

4 Conclusion

Sulfur-modified TiO_2 photocatalysts were synthesized with improved visible-light activity and ability to produce reactive oxygen species. The results reveal that the photocatalytic activity did not depend linearly on the surface sulfur concentration, since S-TiO_2-2 with 1.20×10^{-2} wt% sulfur content shows the highest photocatalytic activity under both UV (ca. 1 g_{HCOOH} g_{cat}^{-1}) and visible light (ca. 0.36 g_{HCOOH} g_{cat}^{-1}) activation. Next, the sulfated TiO_2 with optimized sulfur content was incorporated into polyacrylate-based binder material to prepare a visible-light-active photoreactive composite layer with improved mechanical stability. It was revealed that the binder content of 10 wt% in the hybrid layer did not reduce significantly the photocatalytic activity and the layer also showed an obvious antibacterial effect against *E. coli* bacteria under even relatively low irradiation (1.566 W m^{-2}). This is because of the increased production of hydroxyl radicals by the sulfated TiO_2 (0.296 µmol L^{-1} 7-hydroxycoumarin after 20 min) compared with the unmodified sample (0.083 µmol L^{-1} 7-hydroxycoumarin after 20 min). Therefore, these results indicate that self-cleaning and antimicrobial surfaces can easily be created by surface sulfation and immobilization of photocatalyst particles. Moreover, the surface modification of the initial TiO_2 occurred by simple grinding and calcination with elemental sulfur from desulfurization of petroleum.

Data Availability Statement

Data available on request from the authors.

Supporting Information

Supporting Information for this article can be found under DOI: https://doi.org/10.1002/ceat.202200489. This section includes additional references to primary literature relevant for this research [24, 25].

Acknowledgment

The authors are very thankful for the financial support from the National Research, Development and Innovation Office (GINOP-2.3.2-15-2016-00013 and GINOP-1.1.2-PIACI-KFI-2021-00193). This paper was also supported by the UNKP-22-5 and UNKP-22-4 New National Excellence Program of the Ministry for Innovation and Technology from the source of the National Research, Development and Innovation Fund and by the János Bolyai Research Scholarship of the Hungarian Academy of Sciences. The financial support from Grant 20391-3/2018/FEKUSTRAT of Ministry of Human Capacities, Hungary is also acknowledged (G.F.S.). Á.Á. thanks for the support of the Hungarian NTP-NFTÖ-22-B-0025 scholarship. The authors are grateful to Alexandra N. Kovács for her help in the fluorometric measurements.

The authors have declared no conflict of interest.

Symbols used

A	[m^2]	surface area
c	[mol L^{-1}]	concentration
c_0	[mol L^{-1}]	initial concentration
CFU	[–]	colony-forming unit
E	[eV]	energy
E_g	[eV]	band gap
T	[°C]	temperature

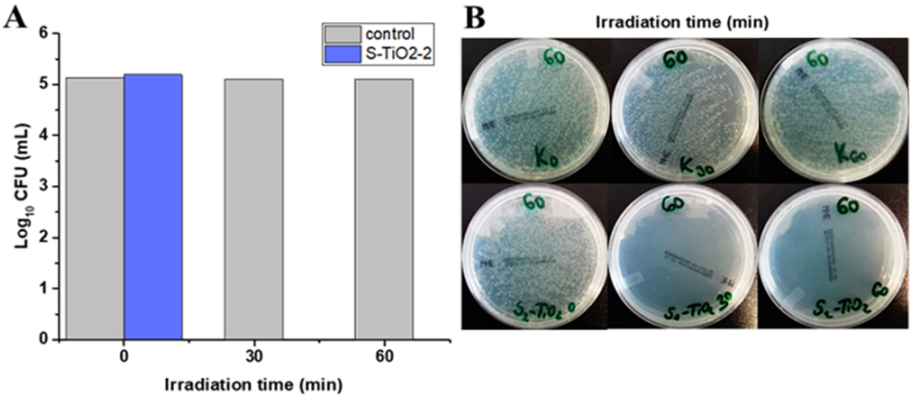

Figure 6. Log_{10} CFU values of *E. coli* ATCC 29522 bacteria as a function of irradiation time at 1.566 W m^{-2} light intensity (A) and the corresponding photographs of bacterial colonies (B).

Greek letters

ζ	[mV]	zeta potential
θ	[°]	diffraction angle
λ	[nm]	wavelength

Abbreviations

BET	Brunauer-Emmett-Teller
DR	diffuse reflectance
EDX	energy-dispersive X-ray
FTIR	Fourier transform infrared
Vis	visible
UV	ultraviolet
XPS	X-ray photoelectron spectroscopy
XRD	X-ray diffraction

References

[1] S. N. Ahmed, W. Haider, *Nanotechnology* **2018**, *29 (34)*, 342001. DOI: https://doi.org/10.1088/1361-6528/aac6ea

[2] Q. Guo, Z. Ma, C. Zhou, Z. Ren, X. Yang, *Chem. Rev.* **2019**, *119 (20)*, 11020–11041. DOI: https://doi.org/10.1021/acs.chemrev.9b00226

[3] M. Humayun, F. Raziq, A. Khan, W. Luo, *Green Chem. Lett. Rev.* **2018**, 86–102. DOI: https://doi.org/10.1080/17518253.2018.1440324

[4] P. L. Sanches, L. R. D. O. Geaquinto, R. Cruz, D. C. Schuck, M. Lorencini, J. M. Granjeiro, A. R. L. Ribeiro, *Front. Bioeng. Biotechnol.* **2020**, *8 (575)*. DOI: https://doi.org/10.3389/fbioe.2020.00575

[5] C. Han, M. Pelaez, V. Likodimos, A. G. Kontos, P. Falaras, K. O'Shea, D. D. Dionysiou, *Appl. Catal. B Environ.* **2011**, *107 (1–2)*, 77–87. DOI: https://doi.org/10.1016/j.apcatb.2011.06.039

[6] X. Hu, Y. Li, J. Tian, H. Yang, H. Cui, *J. Ind. Eng. Chem.* **2017**, *45*, 189–196. DOI: https://doi.org/10.1016/j.jiec.2016.09.022

[7] T. Boningari, S. N. R. Inturi, M. Suidan, P. G. Smirniotis, *Chem. Eng. J.* **2018**, *350*, 324–334. DOI: https://doi.org/10.1016/j.cej.2018.05.122

[8] L. Galeano, S. Valencia, G. Restrepo, J. M. Marín, *Mater. Sci. Semicond. Process.* **2019**, *91*, 47–57. DOI: https://doi.org/10.1016/j.mssp.2018.10.032

[9] V. Kumaravel, S. Mathew, J. Bartlett, S. C. Pillai, *Appl. Catal. B Environ.* **2019**, *244*, 1021–1064. DOI: https://doi.org/10.1016/j.apcatb.2018.11.080

[10] P. K. Sharma, M. A. L. R. M. Cortes, J. W. J. Hamilton, Y. Han, J. A. Byrne, M. Nolan, *Catal. Today* **2019**, *321–322*, 9–17. DOI: https://doi.org/10.1016/j.cattod.2017.12.002

[11] T. Umebayashi, T. Yamaki, H. Itoh, K. Asai, *Appl. Phys. Lett.* **2002**, *81*, 454. DOI: https://doi.org/10.1063/1.1493647

[12] L. G. Devi, R. Kavitha, *Mater. Chem. Phys.* **2014**, *143 (3)*, 1300–1308. DOI: https://doi.org/10.1016/j.matchemphys.2013.11.038

[13] S. Cravanzola, F. Cesano, F. Gaziano, D. Scarano, *Catalysts* **2017**, *7 (7)*, 214. DOI: https://doi.org/10.3390/catal7070214

[14] Z. He, J. Tang, J. Shen, J. Chen, S. Song, *Appl. Surf. Sci.* **2016**, *364*, 416–427. DOI: https://doi.org/10.1016/j.apsusc.2015.12.163

[15] J. B. Gillespie, J. D. Lindberg, L. S. Laude, *Appl. Opt.* **1975**, *14 (4)*, 807–807. DOI: https://doi.org/10.1364/ao.14.000807

[16] M. Náfrádi, L. Farkas, T. Alapi, K. Hernádi, K. Kovács, L. Wojnárovits, E. Takács, *Radiat. Phys. Chem.* **2020**, *170*, 108610. DOI: https://doi.org/10.1016/j.radphyschem.2019.108610

[17] https://www.sigmaaldrich.com/HU/hu/technical-documents/technical-article/analytical-chemistry/photometry-and-reflectometry/ir-spectrum-table (Accessed on June 30, 2021)

[18] A. G. Shard, *Surf. Interface Anal.* **2014**, *46 (3)*, 175–185. DOI: https://doi.org/10.1002/sia.5406

[19] M. C. Biesinger, L. W. M. Lau, A. R. Gerson, R. S. C. Smart, *Appl. Surf. Sci.* **2010**, *257 (3)*, 887–898. DOI: https://doi.org/10.1016/j.apsusc.2010.07.086

[20] C. McManamon, J. O'Connell, P. Delaney, S. Rasappa, J. D. Holmes, M. A. Morris, *J. Mol. Catal. A Chem.* **2015**, *406*, 51–57. DOI: https://doi.org/10.1016/j.molcata.2015.05.002

[21] A. L. Kustov, S. B. Rasmussen, R. Fehrmann, P. Simonsen, *Appl. Catal. B Environ.* **2007**, *76 (1–2)*, 9–14. DOI: https://doi.org/10.1016/J.APCATB.2007.05.004

[22] M. Maicu, M. C. Hidalgo, G. Colón, J. A. Navío, *J. Photochem. Photobiol. A Chem.* **2011**, *217 (2–3)*, 275–283. DOI: https://doi.org/10.1016/J.JPHOTOCHEM.2010.10.020

[23] G. Colón, M. C. Hidalgo, J. A. Navío, *Appl. Catal. B Environ.* **2003**, *45 (1)*, 39–50. DOI: https://doi.org/10.1016/S0926-3373(03)00125-5

[24] J. O. Carneiro, G. Vasconcelos, S. Azevedo, C. Jesus, C. Palha, N. Gomes, V. Teixeira, *Energy Build.* **2014**, *81*, 1–8. DOI: https://doi.org/10.1016/j.enbuild.2014.06.006

[25] Z. Wang, C. Yang, T. Lin, H. Yin, P. Chen, D. Wan, F. Xu, F. Huang, J. Lin, X. Xie, M. Jiang, *Adv. Funct. Mater.* **2013**, *23 (43)*, 5444–5450. DOI: https://doi.org/10.1002/adfm.201300486

